



Contents lists available at ScienceDirect

# Chemical Engineering Science

journal homepage: [www.elsevier.com/locate/ces](http://www.elsevier.com/locate/ces)

## Modeling and control of film porosity in thin film deposition

Gangshi Hu<sup>a</sup>, Gerassimos Orkoulas<sup>a</sup>, Panagiotis D. Christofides<sup>a,b,\*</sup><sup>a</sup>Department of Chemical and Biomolecular Engineering, University of California, Los Angeles, CA 90095, USA<sup>b</sup>Department of Electrical Engineering, University of California, Los Angeles, CA 90095, USA

### ARTICLE INFO

#### Article history:

Received 17 September 2008

Accepted 6 May 2009

Available online 14 May 2009

#### Keywords:

Process control  
 Materials processing  
 Process modeling  
 Process simulation  
 Thin films  
 Model predictive control

### ABSTRACT

Systematic methodologies are developed for modeling and control of film porosity in thin film deposition. The deposition process is modeled via kinetic Monte Carlo (kMC) simulation on a triangular lattice. The microscopic events involve atom adsorption and migration and allow for vacancies and overhangs to develop. Appropriate definitions of film site occupancy ratio (SOR), i.e., fraction of film sites occupied by particles over total number of film sites, and its fluctuations are introduced to describe film porosity. Deterministic and stochastic ordinary differential equation (ODE) models are also derived to describe the time evolution of film SOR and its fluctuation. The coefficients of the ODE models are estimated on the basis of data obtained from the kMC simulator of the deposition process using least-square methods and their dependence on substrate temperature is determined. The developed ODE models are used as the basis for the design of model predictive control (MPC) algorithms that include penalty on the film SOR and its variance to regulate the expected value of film SOR at a desired level and reduce run-to-run fluctuations. Simulation results demonstrate the applicability and effectiveness of the proposed film porosity modeling and control methods in the context of the deposition process under consideration.

© 2009 Elsevier Ltd. All rights reserved.

### 1. Introduction

Currently, there is an increasing need to improve semiconductor manufacturing process operation and yield. This need has arisen due to the increased complexity and density of devices on the wafer, which is the result of increased wafer size and smaller device dimensions. Within this manufacturing environment, thin film microstructure, including thin film surface roughness and amount of internal film defects, has emerged as an important film quality variable which strongly influences the electrical and mechanical properties of microelectronic devices. On one hand, surface roughness of thin films controls the interfacial layer and properties between two successively deposited films. On the other hand, the amount of internal defects, usually expressed as film porosity, plays an important role in determining the thin film microstructure. For example, low-*k* dielectric films of high porosity are being used in current interconnect technologies to meet resistive-capacitive delay goals and minimize cross-talk. However, increased porosity negatively affects the mechanical properties of dielectric films, increasing the risk of

thermo-mechanical failures (Kloster et al., 2002). Furthermore, in the case of gate dielectrics, it is important to reduce thin film porosity as much as possible and eliminate the development of holes close to the interface.

Most of the previous research efforts on modeling and control of thin film microstructure have focused on regulation of thin film surface roughness. This line of research has been motivated by the development of techniques for on-line surface measurement including scanning tunneling microscopy, spectroscopic ellipsometry techniques and grazing-incidence small angle X-ray scattering. Two fundamental modeling approaches, kinetic Monte Carlo (kMC) methods (Gillespie, 1976; Fichtorn and Weinberg, 1991; Shitara et al., 1992; Reese et al., 2001; Christofides et al., 2008) and stochastic differential equation (SDE) models (Edwards and Wilkinson, 1982; Vvedensky et al., 1993; Cuerno et al., 1995; Lauritsen et al., 1996), have been developed to describe the evolution of film microscopic configurations and design feedback control laws. Specifically, kMC models were initially used to develop a methodology for modeling and feedback control of thin film surface roughness (Lou and Christofides, 2003a,b). Successful applications of this control methodology include surface roughness control of: (a) a gallium arsenide (GaAs) deposition process (Lou and Christofides, 2004) and (b) a multi-species deposition process with long range interactions (Ni and Christofides, 2005a). Furthermore, a method that couples partial differential equation (PDE) models and kMC models was developed for computationally

\* Corresponding author at: Department of Chemical and Biomolecular Engineering, University of California, Los Angeles, CA 90095, USA. Tel.: +1 310 794 1015; fax: +1 310 206 4107.

E-mail address: [pdc@seas.ucla.edu](mailto:pdc@seas.ucla.edu) (P.D. Christofides).

efficient multiscale optimization of thin film growth (Varshney and Armaou, 2005). However, kMC models are not available in closed-form and this limitation precludes the use of kMC models for system-level analysis and the design and implementation of model-based feedback control systems. Therefore, it is desirable to achieve better closed-loop performance by designing feedback controllers on the basis of closed-form process models. Linear deterministic models were identified in (Siettos et al., 2003; Armaou et al., 2004; Varshney and Armaou, 2006) from outputs of kMC simulators and were used in controller design using linear control theory. Deterministic models are effective in controlling the expected values of macroscopic variables, which correspond to the first-order statistical moments of the microscopic distribution. However, to control higher statistical moments of the microscopic distributions, such as the surface roughness (the second moment of height distribution on a lattice), deterministic models are not sufficient and SDE models may be needed.

SDEs arise naturally in the modeling of surface morphology of ultra thin films in a variety of material preparation processes (Edwards and Wilkinson, 1982; Villain, 1991; Vvedensky et al., 1993; Cuerno et al., 1995; Lauritsen et al., 1996) since they contain the surface morphology information and account for the stochastic nature of the growth processes. For instance, it has been experimentally verified by atomic force microscopy (AFM) that the Kardar–Parisi–Zhang (KPZ) equation (Kardar et al., 1986) describes satisfactorily the evolution of the surface morphology of GaAs thin films (Ballestad et al., 2002; Kan et al., 2004). However, the construction of SDE models from kMC simulation data or experimental data is a challenging task. Compared to deterministic systems, modeling and identification of dynamical systems of SDEs have received relatively limited attention. Theoretical foundations on the analysis, parameter optimization, and optimal stochastic control for linear stochastic ordinary differential equation (ODE) systems can be found in the early work by Åström (1970). More recently, likelihood-based methods for parameter estimation of stochastic ODE models have been developed (Bohlin and Graebe, 1995; Kristensen et al., 2004). These methods determine the model parameters by solving an optimization problem to maximize a likelihood function or a posterior probability density function of a given sequence of measurements of a stochastic process. Recent results employed statistical moments to reformulate the parameter estimation problem into one involving deterministic differential equations. The stochastic moments include the expected value and variance/covariance obtained from the data set generated by kMC simulations or obtained from experiments. Thus, the issue of parameter estimation of stochastic models could be addressed by employing parameter estimation techniques for deterministic systems. Specifically, following this idea, a method for construction of linear stochastic PDE models for thin film growth was developed and used to construct linear stochastic PDE models for thin film deposition processes in two-dimensional lattices (Ni and Christofides, 2005b). Systematic identification approaches were also developed for linear (Lou and Christofides, 2005a) and non-linear (Hu et al., 2008b) stochastic PDEs and applied to sputtering processes.

Advanced control methods based on SDEs have been developed to address the need of model-based feedback control of thin film microstructure. Specifically, methods for state feedback control of surface roughness based on linear (Lou and Christofides, 2005a,b; Ni and Christofides, 2005b) and nonlinear (Lou and Christofides, 2006; Lou et al., 2008) SDE models have been developed. However, state feedback control assumes full knowledge of the surface morphology at all times, which may be a restrictive requirement in certain practical applications. To this end, output feedback control of surface roughness was recently developed (Hu et al., 2008a) by incorporating a Kalman–Bucy type filter, which utilizes information from a finite number of noisy measurements.

In the context of modeling of thin film porosity, kMC models have been widely used to model the evolution of porous thin films in many deposition processes, such as the molecular beam epitaxial (MBE) growth of silicon films and copper thin film growth (Wang and Clancy, 1998; Zhang et al., 2004). Both monocrystalline and polycrystalline kMC models have been developed and simulated (Levine and Clancy, 2000; Wang and Clancy, 2001). The influence of the macroscopic parameters, i.e., the deposition rate and temperature, on the porous thin film microstructure has also been investigated using kMC simulators of deposition processes. Despite recent significant efforts on surface roughness control, a close study of the existing literature indicates the lack of general and practical methods for addressing the challenging issue of achieving desired electrical and mechanical thin film properties by controlling film porosity to a desired level and reducing run-to-run porosity variability.

Motivated by these considerations, the present work focuses on the development of systematic methodologies for modeling and control of film porosity in thin film deposition processes. Initially, a thin film deposition process which involves atom adsorption and migration is introduced and is modeled using a triangular lattice-based kMC simulator which allows porosity, vacancies and overhangs to develop and leads to the deposition of a porous film. Subsequently, appropriate definitions of film site occupancy ratio (SOR), i.e., fraction of film sites occupied by particles over total number of film sites, and its fluctuation are introduced to describe film porosity. Then, deterministic and stochastic ODE models are derived that describe the time evolution of film SOR and its fluctuation. The coefficients of the ODE models are estimated on the basis of data obtained from the kMC simulator of the deposition process using least-square methods and their dependence on substrate temperature is determined. The developed ODE models are used as the basis for the design of model-predictive control (MPC) algorithms that include penalty on the film SOR and its variance to regulate the expected value of film SOR at a desired level and reduce run-to-run fluctuations. Simulation results demonstrate the applicability and effectiveness of the proposed film porosity modeling and control methods in the context of the deposition process under consideration.

## 2. Thin film deposition process description and modeling

This section is associated with the description of the kMC algorithm of a thin film deposition process. Two microscopic processes are considered; atom adsorption and surface migration. Vacancies and overhangs are allowed in the kMC model to introduce porosity during the thin film growth. Substrate temperature and deposition rate are the macroscopic parameters which control the deposition process.

### 2.1. On-lattice kinetic Monte Carlo model of film growth

The thin film growth process considered in this work includes two microscopic processes: an adsorption process, in which particles are incorporated into the film from the gas phase, and a migration process, in which surface particles move to adjacent sites (Wang and Clancy, 1998, 2001; Levine and Clancy, 2000; Yang et al., 1997). Solid-on-solid (SOS) deposition models, in which vacancies and overhangs are forbidden, are frequently used to model thin film deposition processes (Ni and Christofides, 2005a; Lou and Christofides, 2008) and investigate the surface evolution of thin films. However, vacancies and overhangs must be incorporated in the process model to account for film porosity. Since SOS models are inadequate to model the evolution of thin film internal micro-structure, a ballistic deposition model is chosen to simulate the evolution of film porosity.

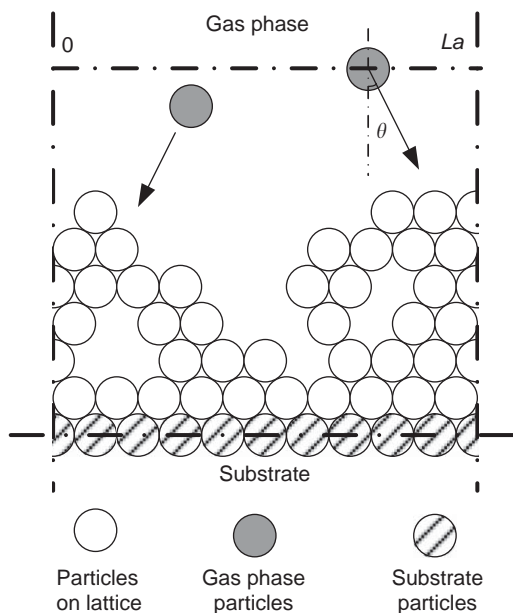


Fig. 1. Thin film growth process on a triangular lattice.

The film growth model used in this work is an on-lattice kMC model in which all particles occupy discrete lattice sites. The on-lattice kMC model is valid for temperatures  $T < 0.5T_m$ , where  $T_m$  is the melting point of the crystal. At high temperatures ( $T \lesssim T_m$ ), the particles cannot be assumed to be constrained on the lattice sites and the on-lattice model is not valid. In this work, a triangular lattice is selected to represent the crystalline structure of the film, as shown in Fig. 1. All particles are modeled as identical hard disks and the centers of the particles deposited on the film are located on the lattice sites. The diameter of the particles equals the distance between two neighboring sites. The width of the lattice is fixed so that the lattice contains a fixed number of sites in the lateral direction. The new particles are always deposited from the top side of the lattice where the gas phase is located; see Fig. 1. Particle deposition results in film growth in the direction normal to the lateral direction. The direction normal to the lateral direction is thus designated as the growth direction. The number of sites in the lateral direction is defined as the lattice size and is denoted by  $L$ . The lattice parameter,  $a$ , which is defined as the distance between two neighboring sites and equals the diameter of a particle (all particles have the same diameter), determines the lateral extent of the lattice,  $La$ .

The number of nearest neighbors of a site ranges from zero to six, the coordination number of the triangular lattice. A site with no nearest neighbors indicates an unadsorbed particle in the gas phase (i.e., a particle which has not been deposited on the film yet). A particle with six nearest neighbors is associated with an interior particle that is fully surrounded by other particles and cannot migrate. A particle with one to five nearest neighbors is possible to diffuse to an unoccupied neighboring site with a probability that depends on its local environment. In the triangular lattice, a particle with only one nearest neighbor is considered unstable and is subject to instantaneous surface relaxation. Details of particle surface relaxation and migration will be discussed in Sections 2.2 and 2.3.

In the simulation, a bottom layer in the lattice is initially set to be fully packed and fixed, as shown in Fig. 1. There are no vacancies in this layer and the particles in this layer cannot migrate. This layer acts as the substrate for the deposition and is not counted in the computation of the number of the deposited particles, i.e., this fixed layer does not influence the film porosity (see Section 3).

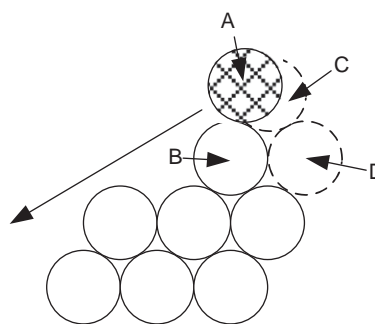


Fig. 2. Schematic of the adsorption event with surface relaxation. In this event, particle A is the incident particle, particle B is the surface particle that is first hit by particle A, site C is the nearest vacant site to particle A among the sites that neighbor particle B, and site D is a stable site where particle A relaxes.

Two types of microscopic processes (Monte Carlo events) are considered, an adsorption process and a migration process. These Monte Carlo events are assumed to be Poisson processes. All events occur randomly with probabilities proportional to their respective rates. The events are executed instantaneously upon selection and the state of the lattice remains unchanged between two consecutive events.

## 2.2. Adsorption process

In an adsorption process, an incident particle comes in contact with the film and is incorporated onto the film. The microscopic adsorption rate,  $W$ , which is in units of layers per unit time, depends on the gas phase concentration. The layers in the unit of adsorption rate are densely packed layers, which contain  $L$  particles. With this definition,  $W$  is independent of  $L$ . In this work, the macroscopic adsorption rate,  $W$ , is treated as a process parameter. For the entire deposition process, the microscopic adsorption rate in terms of incident particles per unit time, which is denoted as  $r_a$ , is related to  $W$  as follows:

$$r_a = LW \quad (1)$$

The incident particles are initially placed at random positions above the film lattice and move toward the lattice in random directions, as shown in Fig. 1. The initial particle position,  $x_0$ , which is the center of an incident particle, is uniformly distributed in the continuous domain,  $(0, La)$ . The incident angle,  $\theta$ , is defined as the angle between the incident direction and the direction normal to the film, with a positive value assigned to the down-right incident direction and a negative value assigned to the down-left incident direction. Probability distribution functions of the incident angle may vary from a Dirac delta function to a cosine function, for different deposition processes. In this work, the probability distribution of the angle of incidence is chosen to be uniform in the interval  $(-0.5\pi, 0.5\pi)$ .

The procedure of an adsorption process is illustrated in Fig. 2. After the initial position and incident angle are determined, the incident particle, A, travels along a straight line toward the film until contacting the first particle, B, on the film. Upon contact, particle A stops and sticks to particle B at the contacting position; see Fig. 2. Then, particle A moves (relaxes) to the nearest vacant site, C, among the neighboring sites of particle B. Surface relaxation is conducted if site C is unstable, i.e., site C has only one neighboring particle, as shown in Fig. 2. When a particle is subject to surface relaxation, the particle moves to its most stable neighboring vacant site, which is defined as the site with the most nearest neighbors. In the case of multiple neighboring vacant sites with the same number of nearest neighbors, a random one is chosen from these sites with equal probability as the objective of the particle surface relaxation process. Note

that particle surface relaxation is considered as part of the deposition event, and thus, it does not contribute to the process simulation time. There is also only one relaxation event per incident particle.

### 2.3. Migration process

In a migration process, a particle overcomes the energy barrier of the site and jumps to its vacant neighboring site. The migration rate (probability) of a particle follows an Arrhenius-type law with a pre-calculated activation energy barrier that depends on the local environment of the particle, i.e., the number of the nearest neighbors of the particle chosen for a migration event. The migration rate of the  $i$ th particle is calculated as follows:

$$r_{m,i} = v_0 \exp\left(-\frac{n_i E_0}{k_B T}\right) \quad (2)$$

where  $v_0$  denotes the pre-exponential factor,  $n_i$  is the number of the nearest neighbors of the  $i$ th particle and can take the values of two to five ( $r_{m,i}$  is zero when  $n_i = 6$  since this particle is fully surrounded by other particles and cannot migrate),  $E_0$  is the contribution to the activation energy barrier from each nearest neighbor,  $k_B$  is Boltzmann's constant and  $T$  is the substrate temperature of the thin film. Since the film is thin, the temperature is assumed to be uniform throughout the film and is treated as a time-varying but spatially invariant process parameter. In this work, the factor and energy barrier contribution in Eq. (2) take the following values  $v_0 = 10^{13} \text{s}^{-1}$  and  $E_0 = 0.6 \text{ eV}$ , which are appropriate for a silicon film (Keršulis and Mitin, 1995).

When a particle is subject to migration, it can jump to either of its vacant neighboring sites with equal probability, unless the vacant neighboring site has no nearest neighbors, i.e., the surface particle cannot jump off the film and it can only migrate on the surface.

### 2.4. Simulation algorithm

After the rates of surface micro-processes are determined, kMC simulations can be carried out using an appropriate algorithm. A comparison between two basic Monte Carlo simulation algorithms, the null-event algorithm (Ziff et al., 1986) and the continuous-time Monte Carlo method (Vlachos et al., 1993), can be found in Reese et al. (2001). The null-event algorithm tries to execute Monte Carlo events on randomly selected sites with certain probabilities, while the continuous-time Monte Carlo (CTMC) method selects an event before the selection of the site on which the event is going to be executed. The existence of null tests makes the null-event algorithm inefficient compared to the CTMC algorithm, especially when the rates of the events are close to 0. In this work, the CTMC method is chosen as the kMC algorithm. With the assumption that all microscopic processes are Poisson processes, the time increment upon the execution of a successful event is computed based on the total rates of all the micro-processes, which can be listed and calculated from the current state of the lattice. To further improve the computational efficiency, a grouping algorithm is also used in the selection of the particle that is subject to migration (Maksym, 1988). In the grouping algorithm, the events are pre-grouped to improve the execution speed. In this work, the layer of the film emerges as a natural grouping criterion, i.e., all particles in the same layer are considered to be part of one group.

With these considerations, the following kMC simulation algorithm is used to simulate the deposition process:

1. A triangular lattice of lateral extent  $La$ , is created to represent the crystalline structure of the film. All particles in the film are constrained to be on the discrete sites of the lattice. A substrate

layer, which is fully packed and fixed, is added at the bottom of the lattice at the beginning ( $t = 0$ ) of the simulation.

2. A list of events is created (or updated) for all possible events including adsorption and migration. The rate for each event is calculated based on the process parameters, i.e., the substrate temperature and the deposition rate.
3. A random number  $\zeta_1 \in (0, r_a + \sum_{i=1}^N r_{m,i})$  is generated to determine whether the next event is an adsorption event ( $0 < \zeta_1 < r_a$ ) or a migration event ( $r_a < \zeta_1 < r_a + \sum_{i=1}^N r_{m,i}$ ), where  $N$  is the total number of deposited particles on the lattice at the specific time instant. Note that the particles being present in the substrate layer are not counted as deposited particles.
4. If the next event is an adsorption event, an incident particle initiates from the gas phase above the film. Two random numbers,  $\zeta_{21} \in (0, La)$  and  $\zeta_{22} \in (-0.5\pi, 0.5\pi)$ , are generated following a uniform probability distribution to determine the initial particle position and incident angle, respectively. The incident particle is incorporated into the film following the microscopic rules for adsorption events discussed in Section 2.2.
5. If the next event is a migration event, a random number  $\zeta_3 \in (0, \sum_{i=1}^N r_{m,i})$  is generated to determine which particle is subject to migration. The migrating particle is found from the following rule:  $\sum_{i=1}^{n-1} r_{m,i} < \zeta_3 < \sum_{i=1}^n r_{m,i}$ , where  $n$  indicates the  $n$ th particle that is subject to migration. The migrating particle jumps to its neighboring vacant site following the microscopic rules for migration events discussed in Section 2.3.
6. Upon the execution of an event, a time increment,  $\delta t$ , is computed by using the following expression:

$$\delta t = -\frac{\ln \zeta_4}{r_a + \sum_{i=1}^N r_{m,i}} \quad (3)$$

where  $\zeta_4$  is a real random number in the  $(0, 1)$  interval.

7. If  $t$  exceeds a preset deposition duration time,  $t_d$ , the kMC simulation is terminated. Otherwise the kMC algorithm is repeated starting from Step 2.

To simulate the process with limited-size lattice and reduce the boundary effects, periodic boundary conditions (PBCs) are applied to the kMC model of the deposition process. Note that PBCs are widely used in molecular level simulations (e.g., Makov and Payne, 1995), so that the statistical properties of a large scale stochastic process can be appropriately captured by kMC simulations carried out on a finite-size lattice.

## 3. Open-loop simulations

In this section, simulations of the kMC model of a silicon thin film growth process using the methodology described in the previous section are presented with the process parameters being kept constant (i.e., open-loop simulation). Appropriate definitions of film site occupancy ratio are also introduced to describe the film porosity and its fluctuation.

### 3.1. Definition of film site occupancy ratio

Since film porosity is the main objective of modeling and control design of this work, a new variable, film site occupancy ratio, is introduced to represent the extent of the porosity inside the thin film as follows:

$$\rho = \frac{N}{LH} \quad (4)$$

where  $\rho$  denotes the film SOR,  $N$  is the total number of deposited particles on the lattice,  $L$  is the lattice size (i.e., number of sites in one layer) and  $H$  denotes the number of deposited layers. Note that

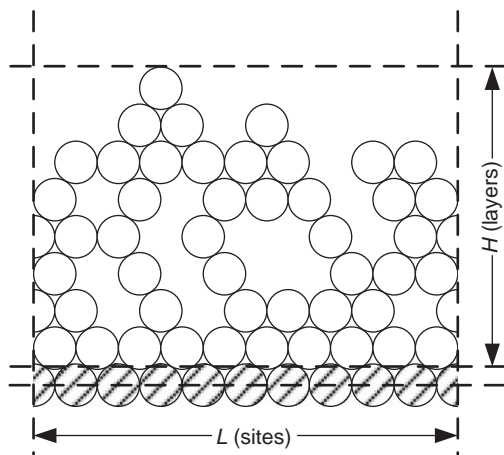


Fig. 3. Illustration of the definition of film SOR of Eq. (4).

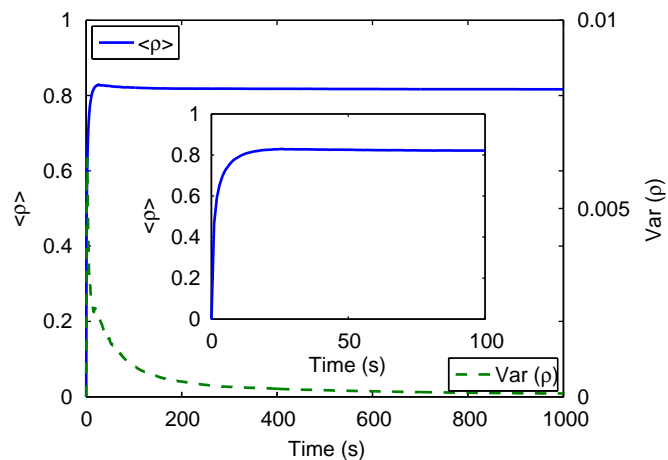


Fig. 4. Mean value (solid lines) and variance (dashed line) of the complete film SOR versus time for a 1000s open-loop deposition process with substrate temperature  $T = 600$  K and deposition rate  $W = 1$  layer/s.

the deposited layers are the layers that contain deposited particles and do not include the initial substrate layer. The concept of packing density, which represents the occupancy ratio of space for a specific packing method, is not the same as the film SOR defined in Eq. (4), and thus, it cannot be used to characterize the evolution of film porosity.

Fig. 3 gives an example showing how film SOR is defined. Since each layer contains  $L$  sites, the total number of sites in the film is  $LH$ . Film SOR is the ratio between the number of deposited particles,  $N$ , and the total number of sites,  $LH$ . With this definition, film SOR ranges from 0 to 1. Specifically,  $\rho = 1$  denotes a film whose sites are fully occupied and has a flat surface. At the beginning of the deposition process when there are no particles deposited on the lattice and only the substrate layer is present,  $N$  and  $H$  are both zeros and the ratio  $N/(LH)$  is not defined, and thus, a zero value is assigned to the film SOR at this state.

Due to the stochastic nature of kMC models of thin film growth processes, the film SOR,  $\rho$ , fluctuates about a mean value,  $\langle \rho \rangle$ , at all times. A quantitative measure of the SOR fluctuations is provided by the variance of the film SOR as follows:

$$\text{Var}(\rho) = \langle (\rho - \langle \rho \rangle)^2 \rangle \quad (5)$$

where  $\langle \cdot \rangle$  denotes the average (mean) value.

### 3.2. Film site occupancy ratio evolution profile

In this subsection, the thin film deposition process is simulated according to the algorithm described in Section 2. The evolution of film SOR and its variance are computed from Eqs. (4) and (5), respectively. The lattice size  $L$  is equal to 100 throughout this work. The choice of lattice size is determined from a balance between statistical accuracy and reasonable requirements for computing power. One thousand independent simulation runs are carried out to obtain the expected value and the variance of the film SOR. The simulation time is 1000 s. All simulations start with an identical flat initial condition, i.e., only a substrate layer is present on the lattice without any deposited particles. Fig. 4 shows the evolution profiles of the expected value and the variance of the film SOR during the deposition process for the following process parameters:  $T = 600$  K and  $W = 1$  layer/s. In Fig. 4, the film SOR is initially 0 and as particles begin to deposit on the film, the film SOR increases with respect to time and quickly reaches a steady-state value. Snapshots of the thin film microstructure at different times,  $t = 100, 400, 700$  and 1000 s, of the open-loop simulation are shown in Fig. 5.

In the snapshots of the microstructure, columnar structures are observed, which is due to the effect of nonlocal shadowing of the existing particles, which prevents incident particles from adsorbing to the film sites that are blocked by the particles at higher positions. Such columnar structures are also observed both in the experiments and in simulations with similar microscopic rules (Wang and Clancy, 1998, 2001; Levine and Clancy, 2000; Zhang et al., 2004). Within the columnar structure, there exist small pores in the microstructure that contribute to the film porosity. Such a structure (columns with few pores) is the result of certain deposition conditions, i.e., the substrate temperature and the adsorption rate considered. Different conditions may result in different microstructure. For example, at the low-temperature region (below 500 K), the deposited thin film shows a tree-like structure with a large number of small pores.

The evolution profile of the variance starts at zero and jumps to a peak, after which the variance decays with respect to time. The variance is used to represent the extent of fluctuation of the film SOR at a given time. Since all simulations start at the same initial condition, the initial variance is zero (by convention) at time  $t = 0$ . As particles begin to deposit on the film, the variance of the film SOR,  $\text{Var}(\rho)$ , increases at short times and it subsequently decreases to zero at large times. Note that the film SOR is a cumulative property since it accounts for all the deposited layers and particles on the film. In other words, the film SOR from each individual simulation run approaches its expected value at large times. Thus, at large times, SOR fluctuations decrease as more layers are included into the film. It is evident from Fig. 4 that the SOR variance decays and approaches zero at large times. Fig. 6 shows the probability distribution functions of the film SOR at different time instants. It can be clearly seen in Fig. 6 that, as time increases, the probability distribution functions become sharper and closer to its mean value, which shows the fact that the fluctuation of film SOR is diminishing (i.e., smaller variance) at large times. Thus, the film SOR of Eq. (4) and its variance of Eq. (5) are not suitable variables for the purposes of modeling and control of film porosity fluctuations. Another variable must be introduced to represent the fluctuation of the film porosity.

### 3.3. Partial film site occupancy ratio

In this subsection, a new concept of film SOR is introduced, termed partial film SOR, which is the film SOR calculated by accounting only for the top  $H_p$  layers of the film. Mathematically, the partial

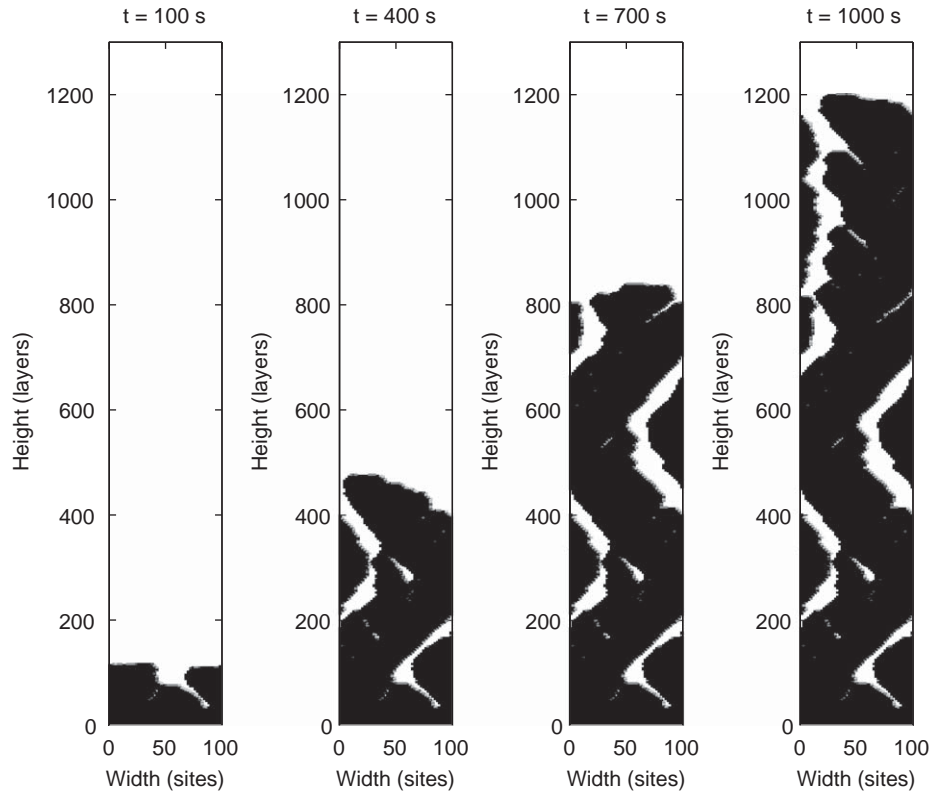


**Fig. 5.** Snapshots of the film microstructure at  $t = 100, 400, 700$  and  $1000$  s of the open-loop deposition process with substrate temperature  $T = 600$  K and deposition rate  $W = 1$  layer/s.

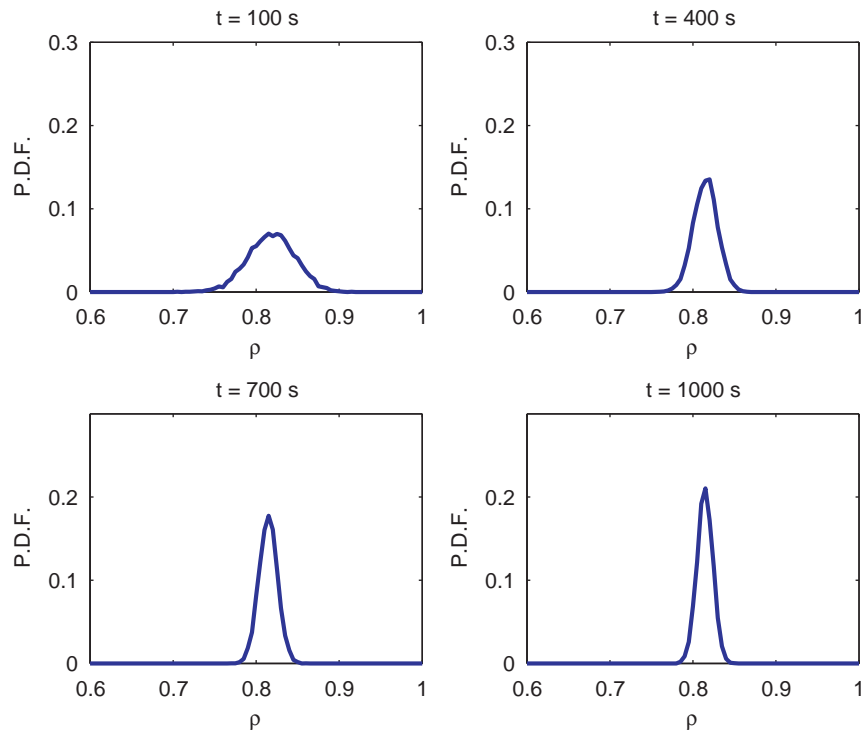


**Fig. 6.** Probability distribution functions (P.D.F.) of film SOR at  $t = 100, 400, 700$  and  $1000$  s of the open-loop deposition process.

film SOR is defined as follows:

$$\rho_p = \frac{N_p}{LH_p} \quad (6)$$

where  $\rho_p$  denotes the partial film SOR and  $N_p$  denotes the number of particles in the top  $H_p$  layers and  $H_p$  denotes the number of top layers of the film included in the computation of the partial film SOR. The definition of the partial film SOR is shown schematically in

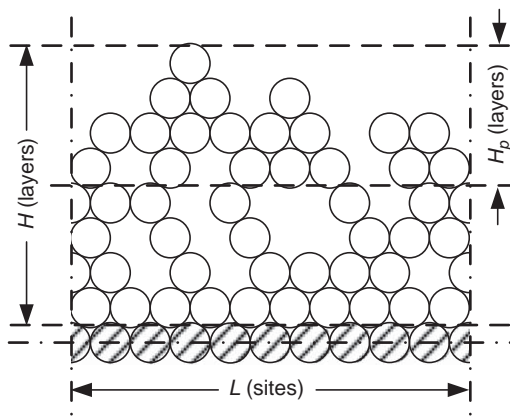


Fig. 7. Illustration of the definition of partial film SOR of Eq. (6).

Fig. 7. To calculate the partial film SOR of Eq. (6), the number of top  $H_p$  layers must first be determined. As shown in Fig. 7, the top  $H_p$  layers start from the top layer of the lattice and include the  $(H_p - 1)$  layers below the top layer. The number of particles in the top  $H_p$  layers is denoted by  $N_p$ . The partial film SOR,  $\rho_p$ , is then calculated as the ratio between  $N_p$  and the total number of sites in the top  $H_p$  layers,  $LH_p$ . Similar to  $\rho$ ,  $\rho_p$  is ranging from 0 to 1.  $\rho_p = 1$  denotes fully occupied top  $H_p$  layers.

The choice of  $H_p$  affects the value of the partial film SOR,  $\rho_p$ , and furthermore, it results in different modeling results and controller performance. Specifically, the partial film SOR cannot be correctly calculated without the existence of  $H_p$  layers in the film. This problem is bypassed by assuming the existence of  $H_p$  fully packed substrate layers in the film before the deposition process begins. These substrate layers are used in the calculation of  $\rho_p$  when  $H < H_p$ . This assumption does not affect the deposition process since the particles in the substrate layers neither migrate nor affect the adsorption or migration processes of the deposited particles. Therefore, at the beginning of deposition, the partial film SOR starts from unity since all  $H_p$  layers are substrate layers and are fully occupied. There also exist alternative choices of  $H_p$  at the beginning of deposition, e.g., equating  $H_p$  with  $H$  and hence having  $\rho_p = \rho$  when  $H < H_p$ . Different choices of  $H_p$  affect the computation of  $\rho_p$  at the initial stages and result in different initial values. However, the main dynamics of the partial film SOR remains unchanged, especially at large times.

Although complete film SOR and partial film SOR are defined similarly, they are different variables, which are used to describe different aspects of the film. The most notable difference is the denominator of the fractions. In the complete film SOR, the denominator of the ratio is the number of the sites in the entire deposited film, and thus, it increases with respect to time, due to the deposition of new particles. This cumulative property of the complete film SOR averages the fluctuations of the porosity from different layers of the film and results in the decay of the variance of the complete film SOR to zero with respect to time. For the partial film SOR, on the contrary, the denominator of the ratio is fixed at  $LH_p$ , and thus,  $\rho_p$  only accounts for the porosity of the newly deposited  $H_p$  layers of the film. Another difference lies in the mechanism of the deposition process. Due to particle migration, particles in the film interior have a higher probability of achieving closed-packed configurations than particles in the top layers. However, newly deposited particles in the top layers have not experienced enough migration events and are more active for migrating. For the above reasons, the fluctuation of  $\rho_p$  does not decay with respect to time and is much larger than the fluctuation of  $\rho$  at large times. Thus, the variance of  $\rho_p$  is selected to represent the porosity fluctuations and is used for modeling and

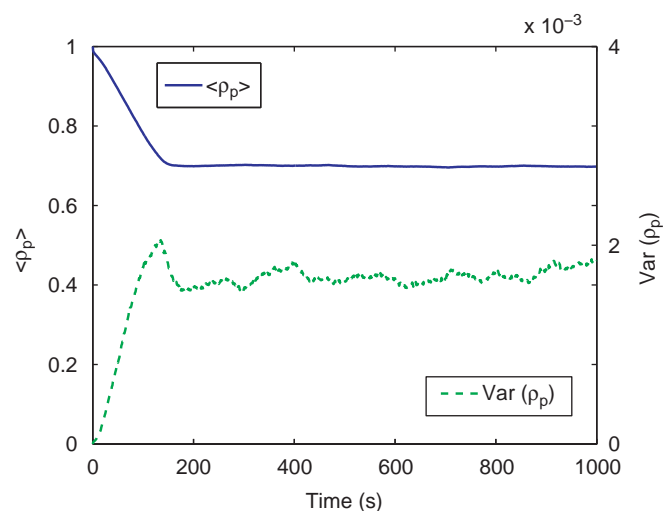


Fig. 8. Mean value (solid line) and variance (dashed line) of the partial film SOR versus time for a 1000 s open-loop deposition process with substrate temperature  $T = 600$  K and deposition rate  $W = 1$  layer/s.

control design. The partial film SOR variance,  $\text{Var}(\rho_p)$ , is computed by the following expression:

$$\text{Var}(\rho_p) = \langle (\rho_p - \langle \rho_p \rangle)^2 \rangle \quad (7)$$

The evolution profiles of the expected partial film SOR and the variance of partial film SOR are shown in Fig. 8 for the same process parameters as in Fig. 4. The top 100 layers are chosen in the calculation of the partial film SOR, i.e.,  $H_p = 100$  in Eq. (6). The choice of  $H_p$  depends on the process requirements. Too few layers result in dramatic fluctuations of the partial film SOR. For a deposition process of about 1000 deposited layers, it is found through extensive simulation tests that 100 top layers constitute a suitable choice for modeling and control design. The magnitude of the variance of the partial film SOR depends on the choice of  $H_p$ . For problems with different lattice sizes, a different  $H_p$  may be selected to produce a representative magnitude of the variance.

As shown in Fig. 8, the mean partial film SOR,  $\langle \rho_p \rangle$ , starts from 1 as a result from the use of the initial substrate layer. Then,  $\langle \rho_p \rangle$  decreases with respect to time and reaches a steady-state value at large times. Compared to the expected film SOR in Fig. 4, the expected partial film SOR is smaller at steady state, since the top layers of the film are newly formed and are more active for particle migration than the bulk layers, which are already deposited for a longer time and are stabilized.

The evolution profile of the variance of partial film SOR,  $\text{Var}(\rho_p)$ , is different from the one of the complete film SOR,  $\text{Var}(\rho)$ , which decays to zero at large times. Similar to the evolution of  $\text{Var}(\rho)$ ,  $\text{Var}(\rho_p)$  starts from zero due to an identical deterministic initial condition applied to all simulations. However,  $\text{Var}(\rho_p)$  does not decay to zero with respect to time, but reaches a steady-state non-zero value. This steady-state non-zero value can be seen from Fig. 9, which shows the probability distribution functions of the partial film SOR at different time instants. As time increases, the probability distribution function of the partial film SOR remains steadily shaped (i.e., steady-state value of variance) instead of becoming sharper as the one of the film SOR shown in Fig. 8. Therefore, the variance of partial film SOR is chosen as the representation of the run-to-run fluctuation of film porosity. Finally, we note that a careful inspection of Figs. 4 and 8 indicates that the variances of the film SOR are two orders of magnitude less than the corresponding mean values, i.e., the mean value of the film SORs  $\sim O(1)$  and the variance of the film SORs  $\sim O(10^{-3})$ .

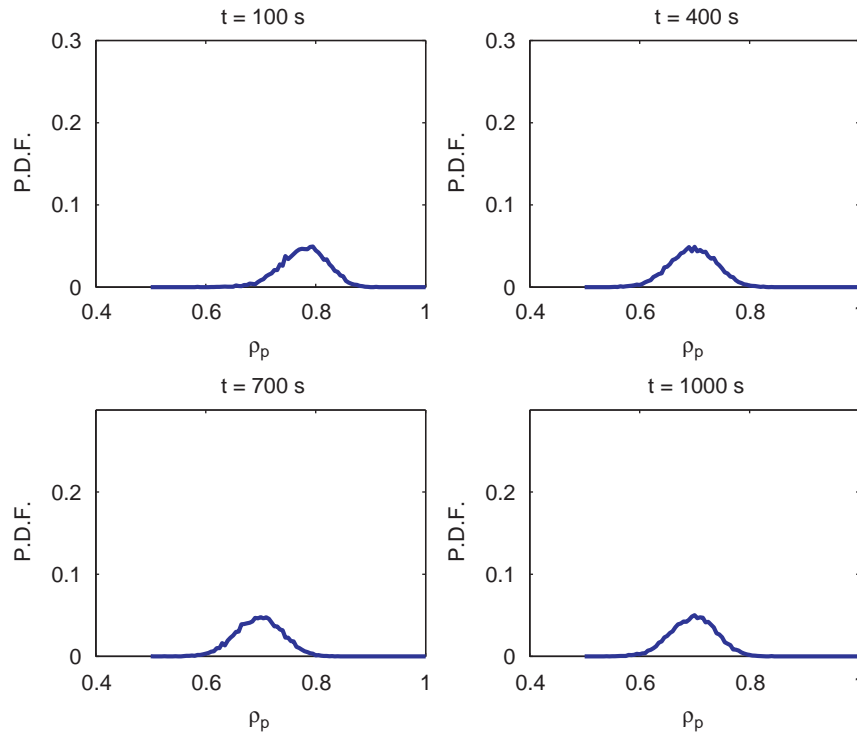


Fig. 9. Probability distribution functions (PDF) of partial film SOR at  $t = 100, 400, 700$  and  $1000$  s of the open-loop deposition process.

#### 4. Construction of ODE models for complete and partial film site occupancy ratio

For control purposes, dynamic models are required that describe how the film porosity expressed in terms of complete and partial film SOR varies with respect to potential manipulated input variables like temperature and deposition rate. In this section, deterministic and stochastic linear ODE models are derived to describe the evolution of film SOR. The derivation of these ODE models and the computation of their parameters is done on the basis of data obtained from the kMC model of the deposition process.

##### 4.1. Deterministic dynamic model of complete film site occupancy ratio

From the open-loop simulation results, the dynamics of the expected value of the complete film SOR evolution can be approximately described by a first-order ODE model. Therefore, a linear first-order deterministic ODE is chosen to describe the dynamics of the complete film SOR as follows:

$$\tau \frac{d\langle\rho(t)\rangle}{dt} = \rho^{ss} - \langle\rho(t)\rangle \quad (8)$$

where  $t$  is the time,  $\tau$  is the time constant and  $\rho^{ss}$  is the steady-state value of the complete film SOR. The deterministic ODE system of Eq. (10) is subject to the following initial condition:

$$\langle\rho(t_0)\rangle = \rho_0 \quad (9)$$

where  $t_0$  is the initial time and  $\rho_0$  is the initial value of the complete film SOR. Note that  $\rho_0$  is a deterministic variable, since  $\rho_0$  refers to the expected value of the complete film SOR at  $t = t_0$ . From Eqs. (8) and (9), it follows that

$$\langle\rho(t)\rangle = \rho^{ss} + (\rho_0 - \rho^{ss})e^{-(t-t_0)/\tau} \quad (10)$$

The model parameters,  $\tau$  and  $\rho^{ss}$ , depend on substrate temperature. This dependence will be mathematically expressed in Section 4.3.

##### 4.2. Stochastic dynamic model of partial film site occupancy ratio

To regulate the variance of the partial film SOR, a stochastic model must be used. For simplicity, a linear stochastic ODE is used to model the dynamics of the partial film SOR. Similar to the deterministic ODE model for the expected complete film SOR of Eq. (8), a first-order stochastic ODE is chosen for the computation of the partial film SOR as follows:

$$\tau_p \frac{d\rho_p(t)}{dt} = \rho_p^{ss} - \rho_p(t) + \xi_p(t) \quad (11)$$

where  $\rho_p^{ss}$  and  $\tau_p$  are the two model parameters which denote the steady-state value of the partial film SOR and the time constant, respectively, and  $\xi_p(t)$  is a Gaussian white noise with the following expressions for its mean and covariance:

$$\begin{aligned} \langle\xi_p(t)\rangle &= 0 \\ \langle\xi_p(t)\xi_p(t')\rangle &= \sigma_p^2\delta(t-t') \end{aligned} \quad (12)$$

where  $\sigma_p$  is a parameter which measures the intensity of the Gaussian white noise and  $\delta(\cdot)$  denotes the standard Dirac delta function. The model parameters  $\rho_p^{ss}$ ,  $\tau_p$  and  $\sigma_p$  are functions of the substrate temperature. We note that  $\xi_p(t)$  is taken to be a Gaussian white noise because the values of  $\rho_p$  obtained from 10,000 independent kMC simulations of the deposition process at large times are in closed accord with a Gaussian distribution law: see Fig. 10 for the histogram of the partial film SOR at  $t = 1000$  s.

The stochastic ODE system of Eq. (11) is subject to the following initial condition:

$$\rho_p(t_0) = \rho_{p0} \quad (13)$$

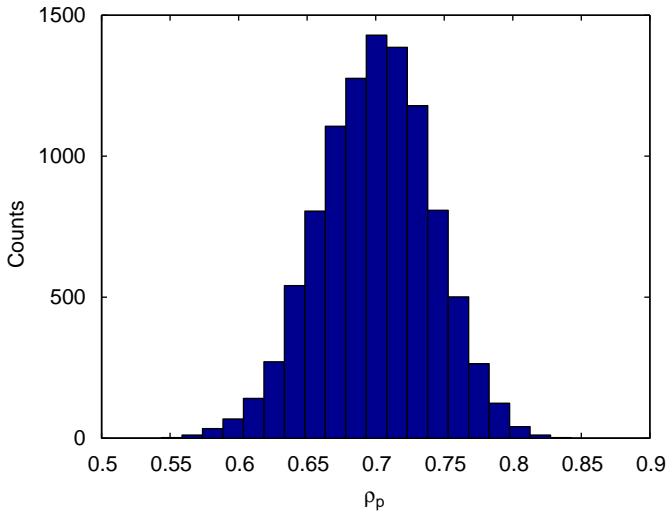


**Fig. 10.** Histogram from 10,000 simulation runs of the partial film SOR at the end ( $t = 1000$  s) of the open-loop deposition process with substrate temperature  $T = 600$  K and deposition rate  $W = 1$  layer/s.

where  $\rho_{p0}$  is the initial value of the partial film SOR. Note that  $\rho_{p0}$  is a random number, which follows a Gaussian distribution.

The following analytical solution to Eq. (11) can be obtained from a direct computation as follows:

$$\rho_p(t) = \rho_p^{ss} + (\rho_{p0} - \rho_p^{ss})e^{-(t-t_0)/\tau_p} + \int_{t_0}^t e^{-(s-t_0)/\tau_p} \zeta_p ds. \quad (14)$$

In Eq. (14),  $\rho_p(t)$  is a random process, the expected value of which,  $\langle \rho_p(t) \rangle$ , can be obtained as follows:

$$\langle \rho_p(t) \rangle = \rho_p^{ss} + (\rho_{p0} - \rho_p^{ss})e^{-(t-t_0)/\tau_p}. \quad (15)$$

The analytical solution of  $\text{Var}(\rho_p)$  can be obtained from the solution to Eq. (14) using the following result (Åström, 1970):

**Result 1.** If (1)  $f(x)$  is a deterministic function, (2)  $\eta(x)$  is a random process with  $\langle \eta(x) \rangle = 0$  and covariance  $\langle \eta(x)\eta(x') \rangle = \sigma^2 \delta(x - x')$ , and (3)  $\varepsilon = \int_a^b f(x)\eta(x) dx$ , then  $\varepsilon$  is a real random variable with  $\langle \varepsilon \rangle = 0$  and variance  $\langle \varepsilon^2 \rangle = \sigma^2 \int_a^b f^2(x) dx$ .

Using Result 1, the variance of the partial film SOR,  $\text{Var}(\rho_p)$ , can be obtained from the analytical solution to Eq. (14) as follows:

$$\text{Var}(\rho_p(t)) = \frac{\tau_p \sigma_p^2}{2} + \left( \text{Var}(\rho_{p0}) - \frac{\tau_p \sigma_p^2}{2} \right) e^{-2(t-t_0)/\tau_p} \quad (16)$$

where  $\text{Var}(\rho_{p0})$  is the variance of the partial film SOR at time  $t = 0$ , which is calculated as follows:

$$\text{Var}(\rho_{p0}) = \langle (\rho_{p0} - \langle \rho_{p0} \rangle)^2 \rangle \quad (17)$$

A new model parameter,  $\text{Var}_p^{ss}$ , is introduced to simplify the solution of  $\text{Var}(\rho_p)$  in Eq. (16) as follows:

$$\text{Var}_p^{ss} = \frac{\tau_p \sigma_p^2}{2} \quad (18)$$

where  $\text{Var}_p^{ss}$  stands for the steady-state value of the variance of the partial film SOR. With the introduction of this new model parameter,

the solution of the variance of the partial film SOR,  $\text{Var}(\rho_p)$ , can be rewritten in the following form:

$$\text{Var}(\rho_p(t)) = \text{Var}_p^{ss} + (\text{Var}(\rho_{p0}) - \text{Var}_p^{ss})e^{-2(t-t_0)/\tau_p} \quad (19)$$

### 4.3. Parameter estimation and dependence on the process parameters

Referring to the deterministic and stochastic ODE models of Eqs. (8) and (11), we note that they include five parameters,  $\rho^{ss}$ ,  $\tau$ ,  $\rho_p^{ss}$ ,  $\tau_p$  and  $\text{Var}_p^{ss}$ . The five parameters describe the dynamics of the film SOR accounting for the effect of fluctuations. These parameters must be estimated by comparing the predicted evolution profiles from the ODE models and the ones from the kMC simulation of the deposition process. Least-square methods are used to estimate the model parameters so that the ODE model predictions are close in a least-square sense to the kMC simulation data.

#### 4.3.1. Parameter estimation

Since the ODE models of Eqs. (8) and (11) are linear, the five parameters,  $\rho^{ss}$ ,  $\tau$ ,  $\rho_p^{ss}$ ,  $\tau_p$  and  $\text{Var}_p^{ss}$ , can be estimated from the solutions to Eqs. (10) and (15). Specifically, the parameters  $\rho_p^{ss}$  and  $\tau_p$  are estimated using Eq. (10) and the parameters  $\rho_p^{ss}$ ,  $\tau_p$  and  $\text{Var}_p^{ss}$  are estimated using Eq. (15), solving two separate least-square problems. Specifically, the two least-square problems can be solved independently to obtain the first four model parameters. The steady-state variance,  $\text{Var}_p^{ss}$ , is obtained from the values of the variance evolution profiles at large times.

The parameters  $\rho^{ss}$  and  $\tau$  are estimated by minimizing the sum of the squared difference between the evolution profiles from the ODE model prediction and the kMC simulation at different time instants as follows:

$$\min_{\rho^{ss}, \tau} \sum_{i=1}^m [(\rho(t_i)) - (\rho^{ss} + (\rho_0 - \rho^{ss})e^{-(t-t_0)/\tau})]^2 \quad (20)$$

where  $m$  is the number of the data pairs,  $(t_i, \langle \rho(t_i) \rangle)$ , from the kMC simulations. Similarly,  $\rho_p^{ss}$  and  $\tau_p$  can be obtained by solving the following least-square optimization problem expressed in terms of the expected partial film SOR:

$$\min_{\rho_p^{ss}, \tau_p} \sum_{i=1}^m [(\rho_p(t_i)) - (\rho_p^{ss} + (\rho_{p0} - \rho_p^{ss})e^{-(t-t_0)/\tau_p})]^2 \quad (21)$$

The data used for the parameter estimation are obtained from the open-loop kMC simulation of the thin film growth process. The process parameters are fixed during each open-loop simulation so that the dependence of the model parameters on the process parameters can be obtained for fixed operation conditions. The complete film SOR and the partial film SOR are calculated on the basis of the deposited film at specific time instants. Due to the stochastic nature of the process, multiple independent simulation runs are performed to obtain the expected values of the complete film SOR and of the partial film SOR as well as of the variance of the partial film SOR.

The above parameter estimation process is applied to the open-loop simulation results. First, the open-loop evolution profiles of the complete film SOR and of the partial film SOR are obtained from 1000 independent kMC simulation runs with substrate temperature  $T = 600$  K and deposition rate  $W = 1$  layer/s. Subsequently, the deterministic and stochastic ODE models of Eqs. (8) and (11) are compared with the open-loop kMC simulation data to compute the model parameters using least-square methods. Figs. 11 and 12 show the open-loop profiles and the predicted profiles of  $\langle \rho \rangle$ ,  $\langle \rho_p \rangle$  and  $\text{Var}(\rho_p)$  from the ODE models with the estimated parameters as follows:

$$\begin{aligned} \rho^{ss} &= 0.8178, & \tau &= 1.6564 \text{ s} \\ \rho_p^{ss} &= 0.6957, & \tau_p &= 77.2702 \text{ s}, & \text{Var}_p^{ss} &= 1.6937 \times 10^{-3} \end{aligned} \quad (22)$$

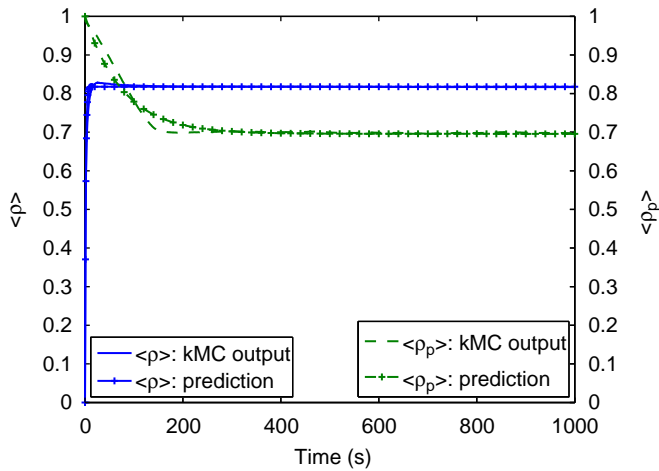


**Fig. 11.** Profiles of the expected value of the complete film SOR (solid line) and of the partial film SOR (dashed line) with respect to time for a 1000 s open-loop deposition process and predictions from the deterministic ODE model (solid line with '+') and the stochastic ODE model (dashed line with '+') with estimated parameters;  $T = 600$  K,  $W = 1$  layer/s.

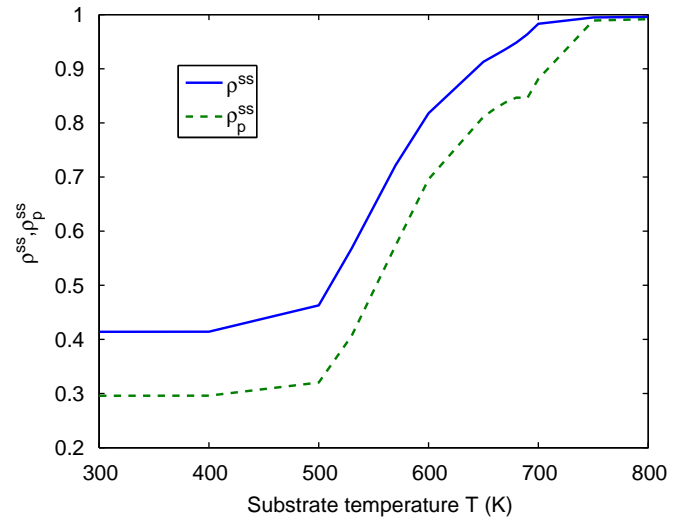


**Fig. 13.** Dependence of  $\rho^{ss}$  and  $\rho_p^{ss}$  on the substrate temperature with deposition rate  $W = 1$  layer/s.

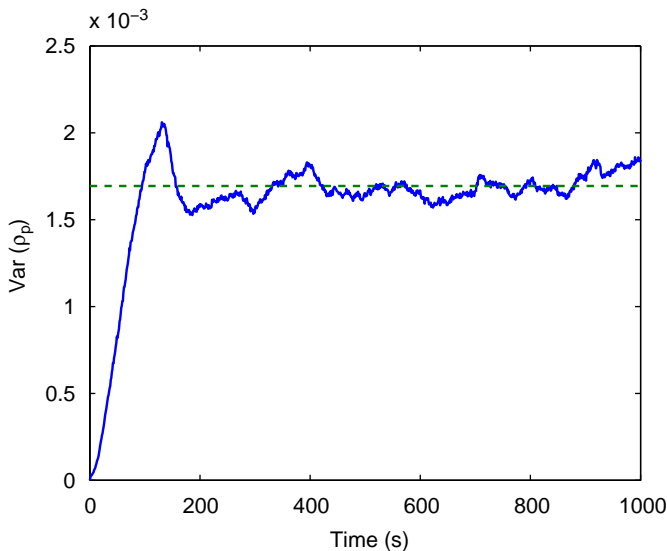


**Fig. 12.** Variance of the partial film SOR with respect to time for a 1000 s open-loop deposition process (solid line) and the estimated steady-state level (dashed line);  $T = 600$  K,  $W = 1$  layer/s.

The predictions from the ODE models are very close to the open-loop kMC simulation profiles, which indicates that the dynamics of the film SOR can be adequately described by first-order ODEs. There is, however, some mismatch of the predicted ODE-based profiles from the kMC data, especially for the expected value of the complete film SOR. This is because the dynamics of the complete film SOR depend on the total height of the film. A film at initial stages is very thin and the complete film SOR changes significantly as more layers are deposited, while a film at large times is much thicker and the complete film SOR is relatively insensitive to the newly deposited layers. Since a first-order ODE model is used to capture the dynamics of the complete film SOR, the time constant,  $\tau$ , is chosen to strike a balance between the initial and final stages of the film growth. Therefore, the predictions from the ODE model cannot match the open-loop profiles, obtained from the kMC models, perfectly at all times. Overall, the computed first-order ODE models approximate

well the dynamics of the film SOR and its fluctuation, and thus, they can be used for the purpose of feedback control design. The closed-loop system simulation results using these first-order models will be discussed in Section 5.3.

The lattice size dependence of the steady-state value of the complete film SOR is shown in Fig. 16. It can be clearly seen that the film SOR depends on the lattice size. To achieve near lattice-size independence, a very large lattice size is required and cannot be simulated using the available amount of computing power. The purpose of the proposed modeling method is to identify the film SOR models from the output of the given deposition process, which can be from either a kMC simulator or experimental deposition process data. Note that the applicability of the proposed modeling method is not limited to any specific lattice size. In this work, a model with lattice size of 100 captures the film SOR dynamics and allows obtaining sufficient statistical accuracy in terms of computing the expected values and variances of film SORs.

#### 4.3.2. Dependence of model parameters on process parameters

The model parameters of the ODE models of Eqs. (8) and (11) depend on two process parameters, temperature and deposition rate. This dependence is used in the formulation of the model predictive control design in the next section when solving the optimization problem. Thus, parameter estimation from open-loop kMC simulation results of the thin film growth process for a variety of process parameters is performed to obtain the relationship between the model parameters and the process parameters. In this work, the deposition rate for all simulations is fixed at 1 layer/s and the only manipulated input considered is the substrate temperature,  $T$ . The range of  $T$  is between 300 and 800 K, which is from room temperature to the upper limit of the allowable temperature for a valid on-lattice kMC model of silicon film. The dependence of the model parameters on the substrate temperature is shown in Figs. 13–15. In these figures, it can be clearly seen that the dependence of the model parameters on temperature is highly nonlinear. For most model parameters, there are asymptotes at the low temperature region due to the limited surface migration rates at low temperatures. However, at high temperatures,  $\rho^{ss}$  and  $\rho_p^{ss}$  approach unity, which corresponds to a fully packed film, i.e., all film sites are occupied by particles.

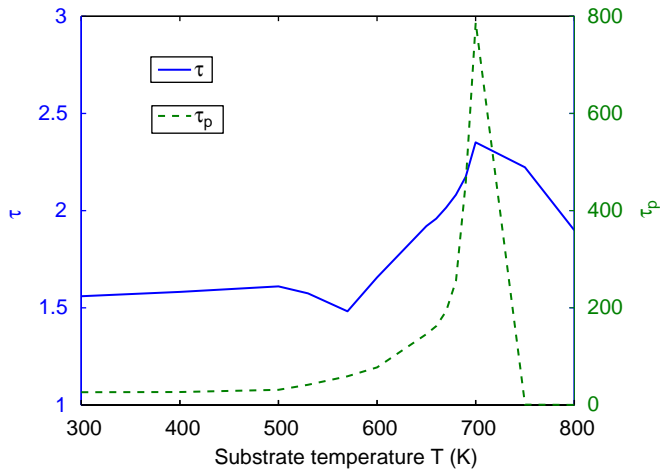


Fig. 14. Dependence of  $\tau$  and  $\tau_p$  on the substrate temperature with deposition rate  $W = 1$  layer/s.

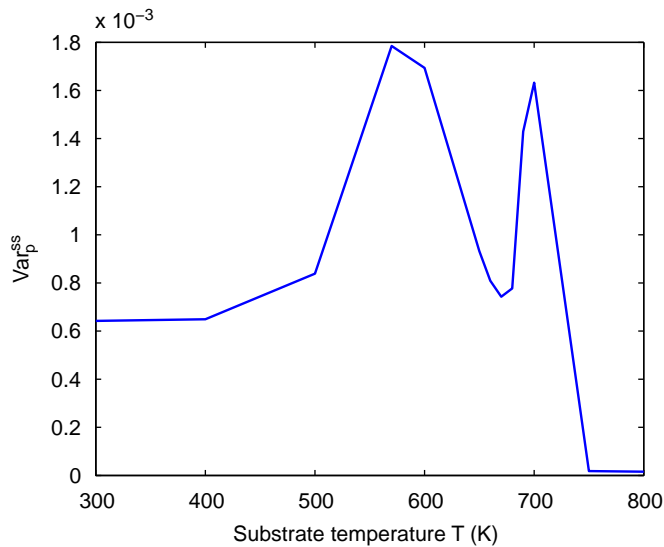


Fig. 15. Dependence of  $\text{Var}_p^{ss}$  on the substrate temperature with deposition rate  $W = 1$  layer/s.

## 5. Model predictive control design

In this section, we design model predictive controllers based on the deterministic and stochastic ODE models of Eqs. (8) and (11) to simultaneously control the complete film SOR of the deposition process to a desired level and minimize the variance of the partial film SOR. State feedback controllers are considered in this work, i.e., the values of the complete film SOR and of the partial film SOR are assumed to be available for feedback control. Real-time film SOR can be estimated from in situ thin film thickness measurements (Buzea and Robbie, 2005) in combination with off-line film porosity measurements.

### 5.1. Regulation of complete film site occupancy ratio

Since the film porosity is the main control objective in this work, we first consider the problem of regulation of the expected complete film SOR to a desired level,  $\rho_{set}$ , within a model predictive control framework. The substrate temperature is used as the ma-

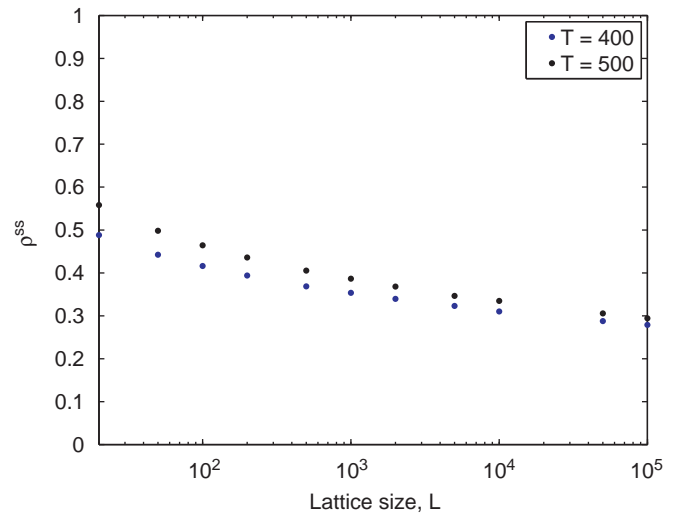


Fig. 16. Dependence of steady-state values of film SOR,  $\rho^{ss}$ , on the lattice size for different temperatures.

nipulated input and the deposition rate is fixed at a certain value,  $W_0$ , during the entire closed-loop simulation. To account for a number of practical considerations, several constraints are added to the control problem. First, there is a constraint on the range of variation of the substrate temperature. This constraint ensures validity of the on-lattice kMC model. Another constraint is imposed on the rate of change of the substrate temperature to account for actuator limitations.

We note that classical control schemes like proportional-integral (PI) control cannot be designed to explicitly account for input/state constraints, optimality considerations and the batch nature of the deposition process, and thus, their use will not be pursued in this work. Furthermore, dynamic open-loop optimization may be used but it does not provide robustness against the model inaccuracies and the fluctuations in the deposition process. In the case where feedback porosity control cannot be attained, dynamic optimization may be used instead; this is naturally included in the proposed model predictive control framework.

The control action, at a time  $t$  and state  $\rho$ , is obtained by solving a finite-horizon optimal control problem. The optimal temperature profile is calculated by solving a finite-dimensional optimization problem in a receding horizon fashion. Specifically, the MPC problem is formulated based on the deterministic ODE of Eq. (8) as follows:

$$\begin{aligned} \min_{T_1, \dots, T_i, \dots, T_p} \quad & J(\rho(t)) = \sum_{i=1}^p q_{sp,i} [\rho_{set} - \langle \rho(t+i\Delta) \rangle]^2 \\ \text{s.t.} \quad & \langle \rho(t+i\Delta) \rangle = \rho^{ss}(T_i, W_0) + (\langle \rho(t+(i-1)\Delta) \rangle \\ & \quad - \rho^{ss}(T_i, W_0)) e^{-\Delta/\tau(T_i, W_0)} \\ & T_{min} < T_i < T_{max} \\ & \left| \frac{T_{i+1} - T_i}{\Delta} \right| \leq L_T \\ & i = 1, 2, \dots, p \end{aligned} \quad (23)$$

where  $t$  is the current time,  $\Delta$  is the sampling time,  $p$  is the number of prediction steps,  $p\Delta$  is the specified prediction horizon,  $T_i$ ,  $i = 1, 2, \dots, p$ , is the substrate temperature at the  $i$ th step ( $T_i = T(t+i\Delta)$ ), respectively,  $W_0$  is the fixed deposition rate,  $q_{sp,i}$ ,  $i = 1, 2, \dots, p$ , are the weighting penalty factors for the error of the complete film SOR at the  $i$ th prediction step,  $T_{min}$  and  $T_{max}$  are the lower and upper bounds on the substrate temperature, respectively, and  $L_T$  is the limit on the rate of change of the substrate temperature. In the MPC formulation of Eq. (23),  $J$  is the cost function, which contains penalty on the

squared difference between the desired value of the complete film SOR,  $\rho_{set}$ , and the predicted values of this variable at all time steps.

The dynamics of the expected value of the complete film SOR are described by the deterministic first-order ODE of Eq. (10). The dependence of model parameters on process parameters is obtained from the parameter estimation at a variety of conditions. Due to the availability of analytical solutions of the linear ODE model of Eq. (10), these analytical solutions can be used directly in the MPC formulation of Eq. (23) for the prediction of  $\langle \rho(t) \rangle$ . The system state,  $\rho(t)$ , is the complete film SOR at time  $t$ . Note that  $\rho(t)$ , which is obtained directly from the simulation in real-time, is considered as the expected complete film SOR and can be used as an initial condition for the solution of the deterministic ODE of Eq. (10). In the closed-loop simulations, the instantaneous values of  $\rho$  and  $\rho_p$  are made available to the controller at each sampling time; however, no statistical information, e.g., the expected value of complete/partial film SOR, is available for feedback. The optimal set of control actions,  $(T_1, T_2, \dots, T_p)$ , is obtained from the solution of the multi-variable optimization problem of Eq. (23), and only the first value of the manipulated input trajectory,  $T_1$ , is applied to the deposition process during the time interval  $(t, t + \Delta)$ . At time  $t + \Delta$ , a new measurement of  $\rho$  is received and the MPC problem of Eq. (23) is solved for the next control input trajectory.

## 5.2. Fluctuation regulation of partial film site occupancy ratio

Reduction of run-to-run variability is another goal in process control of a thin film growth process. In this work, the fluctuation of film SOR is represented by the variance of partial film SOR,  $\text{Var}(\rho_p)$ . Ideally, a zero value means no fluctuation from run to run. However, it is impossible to achieve zero variance of partial film SOR due to the stochastic nature of the thin film growth process. Thus, the control objective of fluctuation regulation is to minimize the variance by manipulating the process parameters.

In this work, the fluctuation is included into the cost function together with the error of the complete film SOR. Specifically, the MPC formulation with penalty on the error of the expected complete film SOR and penalty on the variance of the partial film SOR is given as follows:

$$\min_{T_1, \dots, T_i, \dots, T_p} J(\rho(t)) = \sum_{i=1}^p \{q_{sp,i} [\rho_{set} - \langle \rho(t + i\Delta) \rangle]^2 + q_{var,i} \text{Var}[\rho_p(t + i\Delta)]\} \quad (24)$$

$$\text{s.t. } \langle \rho(t + i\Delta) \rangle = \rho^{ss}(T_i, W_0) + (\langle \rho(t + (i-1)\Delta) \rangle - \rho^{ss}(T_i, W_0))e^{-\Delta/\tau(T_i, W_0)}$$

$$\text{Var}(\rho_p(t + i\Delta)) = \text{Var}_p^{ss}(T_i, W_0) + (\text{Var}[\rho_p(t + (i-1)\Delta)] - \text{Var}_p^{ss}(T_i, W_0))e^{-2\Delta/\tau_p(T_i, W_0)}$$

$$T_{min} < T_i < T_{max} \\ \left| \frac{T_{i+1} - T_i}{\Delta} \right| \leq L_T$$

$$i = 1, 2, \dots, p \quad (25)$$

where  $q_{sp,i}$  and  $q_{var,i}$ ,  $i = 1, 2, \dots, p$ , are weighting penalty factors on the error of the complete film SOR and of the variance of the partial film SOR, respectively. Other variables in Eq. (24) are defined similar to the ones in Eq. (23). The same constraints as in Eq. (23) are imposed on the MPC formulation of Eq. (24). Due to the unavailability of statistical information of the partial film SOR in real-time, the initial condition of the partial film SOR is regarded as a deterministic variable and the initial condition for  $\text{Var}(\rho_p(t))$  is considered to be zero in the MPC formulation.

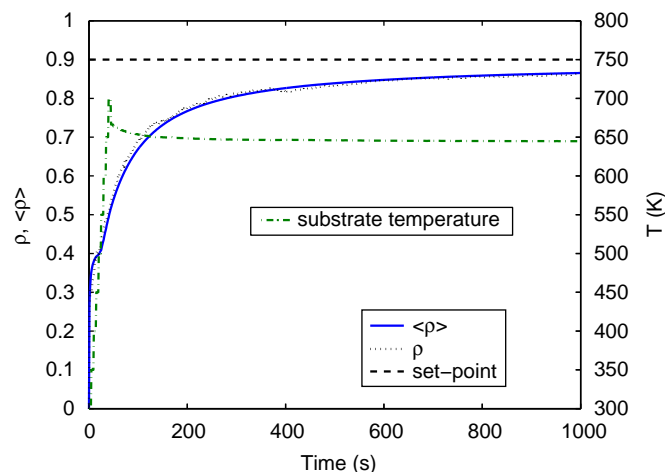


Fig. 17. Closed-loop profiles of the complete film SOR (solid line) and of the expected value of the complete film SOR (dotted line) under the controller of Eq. (23). The profile of the substrate temperature is also included (dash-dotted line).

## 5.3. Closed-loop simulations

In this section, the model predictive controllers of Eqs. (23) and (24) are applied to the kMC model of the thin film growth process described in Section 2. The value of the substrate temperature is obtained from the solution to the problem of Eqs. (23) and (24) at each sampling time and is applied to the closed-loop system until the next sampling time. The complete film SOR and the partial film SOR are obtained directly from the kMC model of the thin film at each sampling time as the state of the system and are fed into the controllers. The sampling time is fixed in all closed-loop simulations to be  $\Delta = 5$  s, which is in the same order of magnitude of the time constant of the dynamics of the complete film SOR,  $\tau$ . The optimization problems in the MPC formulations of Eqs. (23) and (24) are solved using a local constrained minimization algorithm.

The constraint on the rate of change of the substrate temperature is imposed onto the optimization problem, which is realized in the optimization process in the following way:

$$\left| \frac{T_{i+1} - T_i}{\Delta} \right| \leq L_T \Rightarrow |T_{i+1} - T_i| \leq L_T \Delta \Rightarrow T_i - L_T \Delta \leq T_{i+1} \leq T_i + L_T \Delta, \\ i = 1, 2, \dots, p. \quad (26)$$

The desired value (set-point) of the complete film SOR in the closed-loop simulations is 0.9. The number of prediction steps is 5. The deposition rate is fixed at 1 layer/s and all closed-loop simulations are initialized with an initial temperature of 300 K. The maximal rate of change of the temperature is 10 K/s. Expected values and variances are calculated from 1000 independent simulation runs.

### 5.3.1. Regulation of complete film site occupancy ratio

First, the closed-loop simulation results of complete film SOR regulation using the model predictive control formulation of Eq. (23) are provided. In this MPC formulation, the cost function contains only penalty on the difference of the complete film SOR from the set-point value. Specifically, the optimization problem is formulated to minimize the difference between the complete film SOR set-point and the prediction of the expected complete film SOR at the end of each prediction step. All weighting penalty factors,  $q_{sp,i}$ ,  $i = 1, 2, \dots, p$ , are assigned to be equal. Fig. 17 shows the profiles of the expected value of the complete film SOR in the closed-loop system simulation. The profiles of the complete film SOR and of the substrate temperature from a single simulation run are also included in Fig. 17.

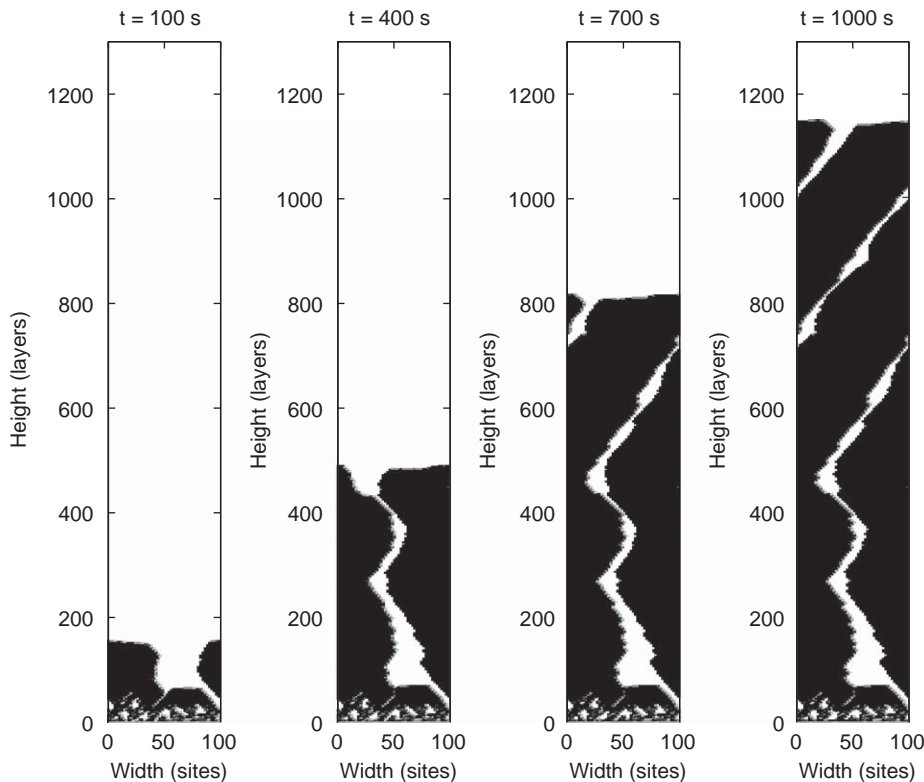


Fig. 18. Snapshots of the film microstructure at  $t = 100, 400, 700$  and  $1000$  s of the closed-loop simulation under the feedback controller of Eq. (23) with  $q_{sp,i} = 1, i = 1, \dots, 5$ .

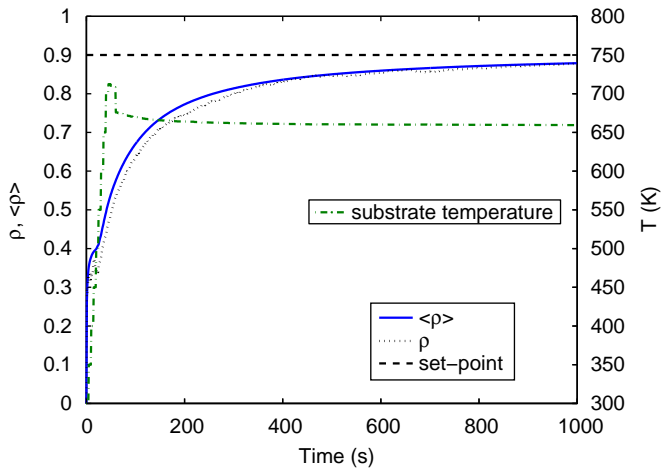


Fig. 19. Closed-loop profiles of the complete film SOR (solid line) and of the expected value of the complete film SOR (dotted line) under the controller of Eq. (24). The profile of the substrate temperature is also included (dash-dotted line).

In Fig. 17, the substrate temperature increases linearly at the initial stages due to the constraint on the rate of change, and it approaches to a value around 650K, which is calculated from the optimization problem based on the current complete film SOR. The expected complete film SOR reaches the value of 0.87 at the end of the simulation. There is a difference of 0.03 from the set point, which is due to the fact that the first-order ODE model is not an exact description of the film SOR dynamics, but rather an approximation. However, for the purpose of control design, the first-order ODE model is acceptable. Another reason for the difference is the cumulative nature of the complete film SOR. Since the initial tem-

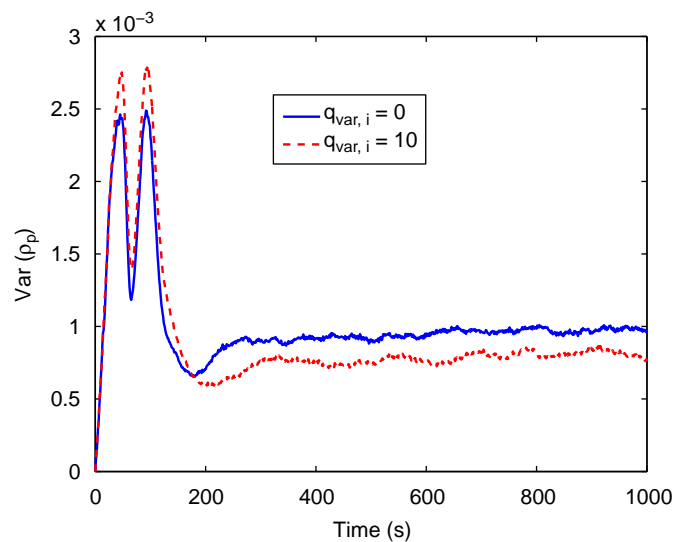
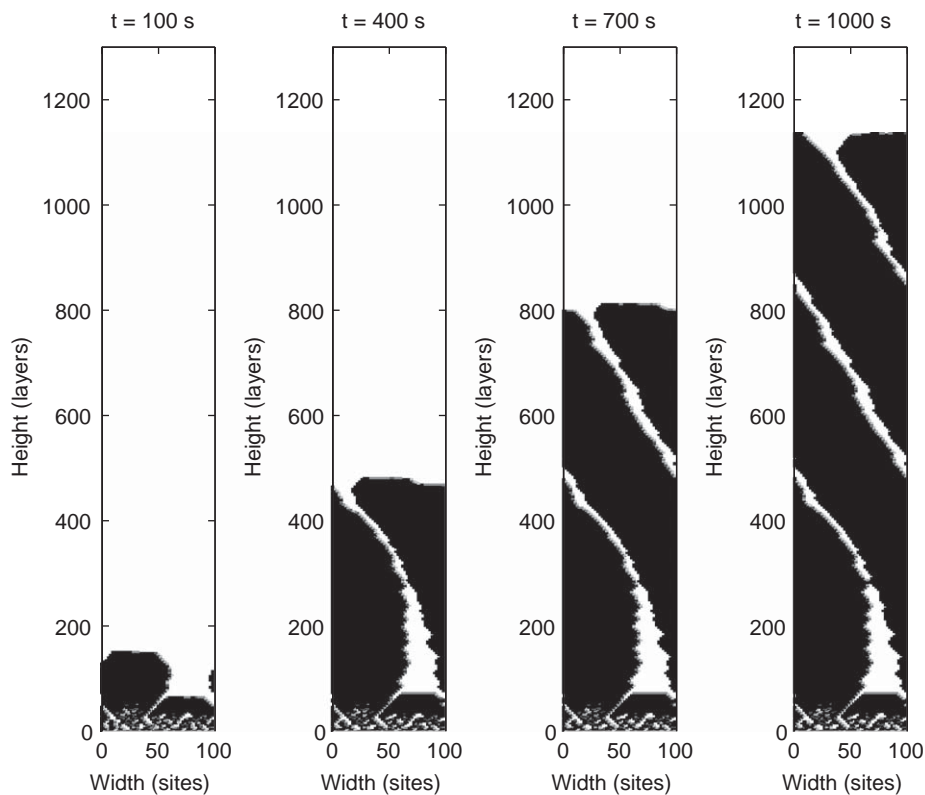


Fig. 20. Comparison of the variance of the partial film SOR for different weights:  $q_{var,i} = 0$  (solid line) and  $q_{var,i} = 10$  (dashed line).

perature, 300K, is far below the optimal temperature for the desired film SOR, it takes some time for the substrate temperature to reach the optimal temperature. The initial condition of the substrate temperature results in a period of low temperature at the initial stages. In this period, layers with higher porosity are deposited onto the film and, as a result, the complete film SOR is lowered. Thus, it takes longer time for the complete film SOR to reach its steady-state value. The difference between the set-point and the closed-loop steady-state value can be overcome by pre-setting a higher initial substrate



**Fig. 21.** Snapshots of the film microstructure at  $t = 100, 400, 700$  and  $1000$  s of the closed-loop simulation under the feedback controller of Eq. (24) with  $q_{sp,i} = 1$ ,  $q_{var,i} = 10$ ,  $i = 1, \dots, 5$ .

temperature. Another possible method to improve the closed-loop performance is to replace the quadratic cost function that penalizes the deviation of the SORs from the desired values with other functions, since quadratic terms slow down the convergence speed in the vicinity of the set point. Snapshots of the film microstructure at different times,  $t = 100, 400, 700$  and  $1000$  s, of the closed-loop simulation are shown in Fig. 18.

### 5.3.2. Fluctuation regulation of partial film site occupancy ratio

To reduce the run-to-run variability of the film porosity, the variance of the partial film SOR is added into the cost function in the model predictive controller of Eq. (24). There are two weighting factors,  $q_{sp,i}$  and  $q_{var,i}$ , which represent the weights on the complete film SOR and on the variance of the partial film SOR prediction, respectively. Fig. 19 shows the profiles of the expected complete film SOR and of the substrate temperature in the closed-loop simulation, with the following values assigned to the weighting factors:

$$q_{sp,i} = 1, \quad q_{var,i} = 10, \quad i = 1-5. \quad (27)$$

As shown in Fig. 19, the complete film SOR and the substrate temperature evolve similarly as in Fig. 17. However, with the cost function including penalty on the variance of the partial film SOR, the optimal temperature is higher than the one in Fig. 17, since a higher substrate temperature is in favor of decreasing run-to-run fluctuations. Fig. 20 shows a comparison of the variance of the partial film SOR between the two model predictive controllers with  $q_{var,i} = 0$  and  $q_{var,i} = 10$ ,  $i = 1-5$ . It can be seen that the variance of the partial film SOR is lowered with penalty on this variable included into the cost function of the MPC formulation. Snapshots of the film microstructure at different times,  $t = 100, 400, 700$  and  $1000$  s, of the closed-loop simulation are shown in Fig. 21.

## 6. Conclusions

In this work, systematic methodologies were developed for modeling and control of film porosity in thin film deposition. A thin film deposition process which involves atom adsorption and migration was introduced and was modeled using a triangular lattice-based kMC simulator which allows porosity, vacancies and overhangs to develop and leads to the deposition of a porous film. Appropriate definitions of film SOR and its fluctuation were introduced to describe film porosity. Deterministic and stochastic ODE models were derived that describe the time evolution of film SOR and its fluctuation. The coefficients of the ODE models were estimated on the basis of data obtained from the kMC simulator of the deposition process using least-square methods and their dependence on substrate temperature was determined. The developed ODE models were used as the basis for the design of MPC algorithms that include penalty on the film SOR and its variance to regulate the expected value of film SOR at a desired level and reduce run-to-run fluctuations. The applicability and effectiveness of the proposed modeling and control methods were demonstrated by simulation results in the context of the deposition process under consideration.

## Acknowledgment

Financial support from NSF, CBET-0652131, is gratefully acknowledged.

## References

- Åström, K.J., 1970. Introduction to Stochastic Control Theory. Academic Press, New York.
- Armaou, A., Siettos, C.I., Kevrekidis, I.G., 2004. Time-steppers and 'coarse' control of distributed microscopic processes. International Journal of Robust and Nonlinear Control 14, 89–111.

- Ballestad, A., Ruck, B.J., Schmid, J.H., Adamczyk, M., Nodwell, E., Nicoll, C., Tiedje, T., 2002. Surface morphology of GaAs during molecular beam epitaxy growth: comparison of experimental data with simulations based on continuum growth equations. *Physical Review B* 65, 205302.
- Bohlin, T., Graebe, S.F., 1995. Issues in nonlinear stochastic grey-box identification. *International Journal of Adaptive Control and Signal Processing* 9, 465–490.
- Buzea, C., Robbie, K., 2005. State of the art in thin film thickness and deposition rate monitoring sensors. *Reports on Progress in Physics* 68, 385–409.
- Christofides, P.D., Armaou, A., Lou, Y., Varshney, A., 2008. *Control and Optimization of Multiscale Process Systems*. Birkhäuser, Boston.
- Cuerno, R., Makse, H.A., Tomassone, S., Harrington, S.T., Stanley, H.E., 1995. Stochastic model for surface erosion via ion sputtering: Dynamical evolution from ripple morphology to rough morphology. *Physical Review Letters* 75, 4464–4467.
- Edwards, S.F., Wilkinson, D.R., 1982. The surface statistics of a granular aggregate. *Proceedings of the Royal Society of London Series A—Mathematical Physical and Engineering Sciences* 381, 17–31.
- Fichthorn, K.A., Weinberg, W.H., 1991. Theoretical foundations of dynamical Monte Carlo simulations. *Journal of Chemical Physics* 95, 1090–1096.
- Gillespie, D.T., 1976. A general method for numerically simulating the stochastic time evolution of coupled chemical reactions. *Journal of Computational Physics* 22, 403–434.
- Hu, G., Lou, Y., Christofides, P.D., 2008a. Dynamic output feedback covariance control of stochastic dissipative partial differential equations. *Chemical Engineering Science* 63, 4531–4542.
- Hu, G., Lou, Y., Christofides, P.D., 2008b. Model parameter estimation and feedback control of surface roughness in a sputtering process. *Chemical Engineering Science* 63, 1800–1816.
- Kan, H.C., Shah, S., Tadyyon-Eslami, T., Phaneuf, R.J., 2004. Transient evolution of surface roughness on patterned GaAs(001) during homoepitaxial growth. *Physical Review Letters* 92, 146101.
- Kardar, M., Parisi, G., Zhang, Y.C., 1986. Dynamic scaling of growing interfaces. *Physical Review Letters* 56, 889–892.
- Keršulis, S., Mitin, V., 1995. Monte Carlo simulation of growth and recovery of silicon. *Material Science & Engineering B* 29, 34–37.
- Kloster, G., Scherban, T., Xu, G., Blaine, J., Sun, B., Zhou, Y., 2002. Porosity effects on low-k dielectric film strength and interfacial adhesion. In: *Proceedings of the IEEE 2002 International Interconnect Technology Conference*. pp. 242–244.
- Kristensen, N.R., Madsen, H., Jorgensen, S.B., 2004. Parameter estimation in stochastic grey-box models. *Automatica* 40, 225–237.
- Lauritsen, K.B., Cuerno, R., Makse, H.A., 1996. Noisy Kuramoto–Sivashinsky equation for an erosion model. *Physical Review E* 54, 3577–3580.
- Levine, S.W., Clancy, P., 2000. A simple model for the growth of polycrystalline Si using the kinetic Monte Carlo simulation. *Modelling and Simulation in Materials Science and Engineering* 8, 751–762.
- Lou, Y., Christofides, P.D., 2003a. Estimation and control of surface roughness in thin film growth using kinetic Monte-Carlo models. *Chemical Engineering Science* 58, 3115–3129.
- Lou, Y., Christofides, P.D., 2003b. Feedback control of growth rate and surface roughness in thin film growth. *A.I.Ch.E. Journal* 49, 2099–2113.
- Lou, Y., Christofides, P.D., 2004. Feedback control of surface roughness of GaAs (001) thin films using kinetic Monte-Carlo models. *Computers & Chemical Engineering* 29, 225–241.
- Lou, Y., Christofides, P.D., 2005a. Feedback control of surface roughness in sputtering processes using the stochastic Kuramoto–Sivashinsky equation. *Computers & Chemical Engineering* 29, 741–759.
- Lou, Y., Christofides, P.D., 2005b. Feedback control of surface roughness using stochastic PDEs. *A.I.Ch.E. Journal* 51, 345–352.
- Lou, Y., Christofides, P.D., 2006. Nonlinear feedback control of surface roughness using a stochastic PDE: design and application to a sputtering process. *Industrial & Engineering Chemistry Research* 45, 7177–7189.
- Lou, Y., Hu, G., Christofides, P.D., 2008. Model predictive control of nonlinear stochastic partial differential equations with application to a sputtering process. *A.I.Ch.E. Journal* 54, 2065–2081.
- Makov, G., Payne, M.C., 1995. Periodic boundary conditions in ab initio calculations. *Physical Review B* 51, 4014–4022.
- Maksym, P.B., 1988. Fast Monte Carlo simulation of MBE growth. *Semiconductor Science and Technology* 3, 594–596.
- Ni, D., Christofides, P.D., 2005a. Dynamics and control of thin film surface microstructure in a complex deposition process. *Chemical Engineering Science* 60, 1603–1617.
- Ni, D., Christofides, P.D., 2005b. Multivariable predictive control of thin film deposition using a stochastic PDE model. *Industrial & Engineering Chemistry Research* 44, 2416–2427.
- Reese, J.S., Raimondeau, S., Vlachos, D.G., 2001. Monte Carlo algorithms for complex surface reaction mechanisms: efficiency and accuracy. *Journal of Computational Physics* 173, 302–321.
- Shitara, T., Vvedensky, D.D., Wilby, M.R., Zhang, J., Neave, J.H., Joyce, B.A., 1992. Step-density variations and reflection high-energy electron-diffraction intensity oscillations during epitaxial growth on vicinal GaAs(001). *Physical Review B* 46, 6815–6824.
- Siettos, C.I., Armaou, A., Makeev, A.G., Kevrekidis, I.G., 2003. Microscopic/stochastic timesteppers and “coarse” control: a kMC example. *A.I.Ch.E. Journal* 49, 1922–1926.
- Varshney, A., Armaou, A., 2005. Multiscale optimization using hybrid PDE/kMC process systems with application to thin film growth. *Chemical Engineering Science* 60, 6780–6794.
- Varshney, A., Armaou, A., 2006. Identification of macroscopic variables for low-order modeling of thin-film growth. *Industrial & Engineering Chemistry Research* 45, 8290–8298.
- Villain, J., 1991. Continuum models of crystal growth from atomic beams with and without desorption. *Journal de Physique I* 1, 19–42.
- Vlachos, D.G., Schmidt, L.D., Aris, R., 1993. Kinetics of faceting of crystals in growth, etching, and equilibrium. *Physical Review B* 47, 4896–4909.
- Vvedensky, D.D., Zangwill, A., Luse, C.N., Wilby, M.R., 1993. Stochastic equations of motion for epitaxial growth. *Physical Review E* 48, 852–862.
- Wang, L., Clancy, P., 1998. A kinetic Monte Carlo study of the growth of Si on Si(100) at varying angles of incident deposition. *Surface Science* 401, 112–123.
- Wang, L., Clancy, P., 2001. Kinetic Monte Carlo simulation of the growth of polycrystalline Cu films. *Surface Science* 473, 25–38.
- Yang, Y.G., Johnson, R.A., Wadley, H.N., 1997. A Monte Carlo simulation of the physical vapor deposition of nickel. *Acta Materialia* 45, 1455–1468.
- Zhang, P., Zheng, X., Wu, S., Liu, J., He, D., 2004. Kinetic Monte Carlo simulation of Cu thin film growth. *Vacuum* 72, 405–410.
- Ziff, R.M., Gulari, E., Barshad, Y., 1986. Kinetic phase transitions in an irreversible surface-reaction model. *Physical Review Letters* 56, 2553–2556.